Biosensors and Bioelectronics 68 (2015) 633–641

Contents lists available at ScienceDirect

Biosensors and Bioelectronics

journal homepage: www.elsevier.com/locate/bios

Self assembled DC sputtered nanostructured rutile TiO_2 platform for bisphenol A detection

Nawab Singh [a,b], K. Kamil Reza [a], Md. Azahar Ali [a], Ved Varun Agrawal [a,*], A.M. Biradar [a]

[a] Centre on Biomolecular Electronics, Biomedical Instrumentation Section, CSIR-National Physical Laboratory, Dr. K. S. Krishnan Marg, New Delhi 110012, India

[b] Biomedical Engineering, Indian Institute of Technology Hyderabad, Ordnance Factory Estate, Yeddumailaram 502205, Andhra Pradesh, India

ARTICLE INFO

Article history:
Received 17 September 2014
Received in revised form
31 December 2014
Accepted 19 January 2015
Available online 22 January 2015

Keywords:
DC sputtering
Electrochemical oxidation
Nanocrystalline titanium
Nanostructured TiO_2
Bisphenol A
Tyrosinase
APTES

ABSTRACT

A novel biosensor platform comprising of the functionalized sputtered rutile nanostructured titanium dioxide ($nTiO_2$) for rapid detection of estrogenic substance (bisphenol A) has been proposed. The direct current (DC) sputtering of titanium (Ti) on glass substrate has been converted to ordered nanostructured TiO_2 film via oxidation. The nanostructured TiO_2 surface was functionalized with self-assembled monolayer (SAM) of 3-aminopropyltriethoxysilane (APTES) and glutaraldehyde. The enzyme molecule, tyrosinase (Tyrs) has been covalently immobilized on the surface of APTES modified nanostructured TiO_2 film. To investigate the crystalline structure and surface morphology of functionalized $nTiO_2$/Ti electrode, the X-ray diffraction, scanning electron microscopy, atomic force microscopy and Fourier transform infrared spectroscopy have been carried out. This impedimetric biosensor exhibits a comparable sensitivity (361.9 kΩ/μM) in a wide range of detection (0.01–1.0 μM) and a response time of 250 s for bisphenol A (BPA) monitoring. This novel manufacturing process for $nTiO_2$ film is cheap, practical and safer for functionalization with SAM and glutaraldehyde to improve the biosensor efficacy. The strong protein absorption capability of the $nTiO_2$ surface demonstrates an excellent electrochemical biosensor and could be useful for the detection of other phenolic compounds.

1. Introduction

Endocrine-disrupting chemicals (EDCs) are known as substances that discharge natural hormones in the human endocrine system, thus causing undesirable effects on human body and animal (Kloas et al., 1999; Yin et al., 2010; Vandenberg et al., 2012; WHO, 2012). The EDCs include bisphenol A (BPA), 2,2-bis (4-hydroxyphenyl) propane, etc. that exhibits estrogenic activity in the human body even at very low concentrations (Sohoni et al., 2001; Steinmetz et al., 1997). EDCs can interfere with the endocrine system of both the human and animal resulting in cancer diseases, decrease semen quality, reduce immune function and impair reproduction (Hiroi et al., 1999; Wang et al., 2014; DiVall, 2013). BPA is a raw material (monomer) for the synthesis of epoxy resins (EP), polystyrene resins (PS), polycarbonate (PC) plastics, flame retardants, and other specialty products which are widely used for inner coating of food cans, water bottles, dental sealants, food packaging and drug delivery systems (Ntsendwana et al., 2012; Yin et al., 2010). BPA can directly release to water surface during manufacturing and processing in industries. Thus, there is an urgent need for degradation and detection of these chemicals contaminations. The detection of BPA is an important for both biomedical diagnostics and environmental monitoring (Alkasir et al., 2010). Various techniques have been employed for the determination of BPA in environment such as high-performance liquid chromatography, gas chromatography (Wen et al., 2006), capillary electrophoresis and solid phase microextraction. These techniques are time consuming, complex procedure, expensive and require large sample volumes. In this context, the electrochemical biosensor offers several advantages such as fast detection, simple, inexpensive and in situ real-time monitoring (Alkasir et al., 2010; Apocada et al., 2011; Reza et al., 2014).

Titanium (Ti) and titanium dioxide (TiO_2) are exciting materials and widely explored in the development of bio-electronic devices due to its unique properties. Ti has been used to create artificial hips, pins for setting bones, bone-anchoring device, dental implant, heart-valve and cardiac pacemakers (Brown and Lemons, 1996; Kim and Ramaswamy, 2009). In addition, Ti substrate can be a good choice for biosensor material. However, Ti substrate has a major concern for fabrication of biosensor due to its lack of biomolecules absorption on its surface resulting from weak electrostatic interaction with biomolecules. To overcome this problem, Ti

* Corresponding author.
E-mail address: ved.varun@gmail.com (V.V. Agrawal).

http://dx.doi.org/10.1016/j.bios.2015.01.041
0956-5663/

surface can be modified using electrochemical oxidation which can convert uniformly the Ti surface into porous TiO_2. The electrochemical oxidation is an effective way to prepare bioactive TiO_2 film in presence of hydrofluoric acid (HF) and ethyleneglycol (Zhou et al., 2012). Nanostructured titanium dioxide ($nTiO_2$) is an attractive material which provides a suitable interface for proteins immobilization for development of biosensor due to their advanced properties such as large specific surface area and strong adsorption ability. The surface morphology of $nTiO_2$ can be tuned by controlling the oxidation conditions such as voltage, electrolyte concentration and pH etc. TiO_2 has been widely used in photocatalysts, solid-state solar cells, organic synthesis, battery and biosensor applications. The $nTiO_2$ exhibits excellent biocompatibility, non-toxicity, surface functionality, and porous morphology for biomolecules attachment (Ali et al., 2012). $nTiO_2$ is a good candidate for biosensor material due to its excellent electron transport properties. It can undergo various chemical and physical functionalizations to produce suitable surface for the adsorption of organic and biological molecules. DC sputtered $nTiO_2$ electrode may improve absorption ability of biomolecules resulting in higher sensitivity and detection limit of the biosensor.

TiO_2 is known to exist in three crystalline structures such as rutile (tetragonal), brookite (orthorhombic) and anatase (tetragonal). The anatase phase of TiO_2 has been widely used in biosensor application due to its good stability and reactive facets. The application of rutile TiO_2 in biosensor is not much explored due to high transition temperature from anatase to rutile phase. In this context, low temperature synthesis of nanostructured rutile TiO_2 play an important role in the fabrication of biosensor. Oxygen vacancies and hydroxyl groups in rutile $nTiO_2$ are known as point defects, and their electron-trapping nature has been investigated by density functional calculation (Di Valentin et al., 2006). Besides this, surface defects including step edges, oxygen vacancies, line defects, impurities and crystallographic trim planes can improve the electrocatalytic activity and charge transfer properties. In particular, oxygen vacancies in conjunction with the conversion of Ti^{4+} to Ti^{3+} and located within the bridging oxygen rows of the TiO_2 (110)–(1×1) surface that can be achieved using ion sputtering and electron beam bombardment (Guillemot et al., 2002). The creation of Ti^{3+} defects has a potential effect on the electronic properties of electrode surface. The Ti^{3+} defects in $nTiO_2$ provide the active adsorption sites for enzymes or proteins and improve the electron transfer rate between electrode and electrolyte (Xiao et al., 2011). Xiao et al. (2011) have explained the effect of surface defects for $nTiO_2$ in biosensing. It has been found the electron transfer properties and enzyme adsorption of $nTiO_2$ improved largely due to dissociative absorption of water by Ti^{3+} defects. Berger et al. (2007) have investigated the electrochemical properties on the nature of trap states in the rutile $nTiO_2$ film. Besides this, the self-assembled monolayer (SAM) plays a major role for immobilization of enzyme molecules on $nTiO_2$. On $nTiO_2$ surface, SAM has recently found to be much attraction in the development of bio-molecular electronic devices due to its stronger bond formation (Oliveira et al., 2007). Thus, this low temperature process for manufacturing $nTiO_2$ film is suitable to provide easy, cheap and safer for SAM and glutaraldehyde in order to enhance biosensor characteristics.

In this work, we have deposited the Ti film on glass substrate using DC sputtering technique. The Ti film has been converted to rutile TiO_2 nanostructure through electrochemical oxidation in presence of hydrofluoric acid and ethylene glycol. SAM of APTES has been treated on rutile $nTiO_2$ film surface to perform cross link with glutaraldehyde molecules. For impedimetric detection of BPA, tyrosinase enzyme has been covalently immobilized on APTES-$nTiO_2$/Ti electrode surface. Fabricated biosensor has been utilized to detect various concentrations of BPA using electrochemical impedance spectroscopic technique.

2. Materials and methods

2.1. Fabrication of sputtered titanium film

Ti film was deposited onto glass substrate by direct current (DC) magnetron sputter coater (MILMAN®, India) using titanium target (99.99% pure, 3 in. diameter and 5-mm thick). For sputtering, the glass substrates were initially cleaned with soap solution, thereafter were rubbed with lint free wipe and rinsed in double distilled water. Then, the glass substrates were kept for ultrasonication for 10 min in warm acetone solution at ~55 °C and dried in compressed nitrogen gas. Ti films were sputtered in argon plasma at a pressure of 5×10^{-6} mTorr (mT). During deposition, the deposition time was kept for 2 min and target–substrate distance was maintained as 70 mm.

2.2. Electrochemical oxidation

The layer of nanostructured titanium dioxide ($nTiO_2$) film has been grown onto Ti film via electrochemical oxidation. Surface of Ti film was converted into $nTiO_2$ film in presence of ethylene glycol and HF solution via oxidation at 35 V for 180 s. Ti/glass electrode was placed at anode and a platinum electrode used as a counter electrode (Fig. S1, Supplementary data). The distance between the Ti and counter electrode was maintained at 0.8 cm for deposition. The pH of the electrolyte solution was maintained at 4.5 using HNO_3 and $NH_3\cdot H_2O$. After oxidation, the film was rinsed with deionised water and dried under nitrogen. The oxidized crystalline TiO_2 film was further annealed at 95 °C for 3 h in order to remove any residue.

2.3. Biosensing platform

For immobilization of enzyme, the fabricated $nTiO_2$/Ti electrode was modified by self-assembled monolayer (SAM) of APTES and further GA was immobilized as a cross linker. The silanization of $nTiO_2$/Ti electrode was performed by incubation at room temperature (25 °C) for 18 h in dry toluene containing APTES (1%) solution to form an aminosilane monolayer. Silane groups of APTES can interact with $nTiO_2$/Ti electrode to form Si–O–Ti bond on electrode surface. Remaining active amino groups of APTES can react readily with cross linker GA to form aldehyde group on electrode surface. The film was consequently rinsed with toluene and DI water to remove any physically absorbed aminosilane and then dried at room temperature. For immobilization, 10 μl of tyrosinase (Tyrs) enzyme solution was spread uniformly on APTES-$nTiO_2$/Ti electrode surface and stored it at 4 °C for 12 h. GA was used as a cross linker in between Tyrs enzyme and APTES. The amine groups in Tyrs interact with carbonyl groups of GA to form amide bonds on electrode surface (Weetall and Hersh, 1970).

3. Results and discussion

3.1. Structural properties

Fig. 1 shows X-ray diffraction (XRD) patterns of Ti and $nTiO_2$ films. The characteristic diffraction peaks of Ti film at $2\theta=34.95$ and 37.90 corresponding to (100) and (002) (JCPDS file 89-2762) reflection planes of hexagonal close packed (hcp) crystal structure (Dunn et al., 2001; Li et al., 2005). The crystallite size is estimated as ~20 nm for (d_{002}) reflection plane using the Scherrer formula. Fig. 1 (curve b) shows the diffraction peaks at $2\theta=29.09$, 35.66,

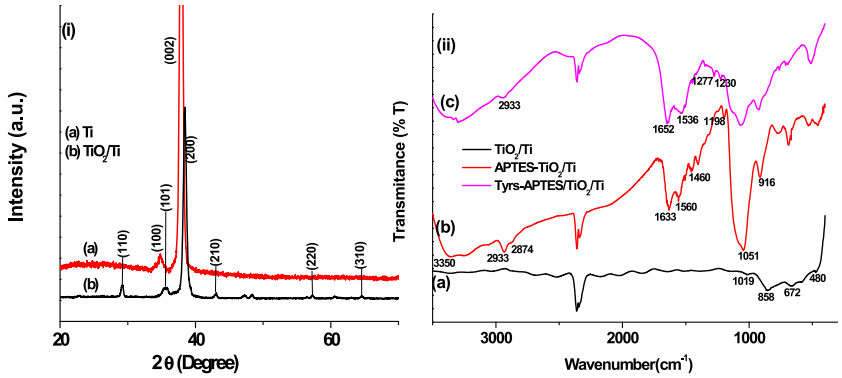

Fig. 1. (i) X-ray diffraction pattern of Ti film (a) and nanostructured TiO_2 film (b) (ii). FTIR spectra of $nTiO_2$/Ti electrode (a), APTES-$nTiO_2$/Ti electrode (b) and Tyrs–APTES/$nTiO_2$/Ti bio electrode (c).

38.46, 43.13, 57.28 and 64.62 corresponding to characteristic reflection planes (110), (101), (200), (210), (220) and (310) of $nTiO_2$, (JCPDS file 82-0514, 21-1276), that confirm a transition from metallic phase of Ti to rutile phase TiO_2 film (Scheme 1, Supplementary data). The estimated crystallite size for (200) plane of $nTiO_2$ films is obtained as ~18 nm, which is slightly lesser than calculated crystallite size of Ti.

Typical Fourier transform infrared (FTIR) spectra of $nTiO_2$ film and surface modified films are shown in [Fig. 1(ii)]. The FTIR spectra of $nTiO_2$ film (curve a) shows the absorption bands at 480, 672 and 858 cm^{-1} in the finger print region due to the vibrations of Ti–O and Ti–O–Ti framework bonds of the rutile phase of $nTiO_2$ (Duenas et al., 2005). However, this film shows the additional peaks at 1051 and 1198 cm^{-1} after immobilization of APTES and GA on $nTiO_2$/Ti (curve b) surface due to vibration of $Si–OCH_2CH_3$ bond that confirm the siloxane bond formation between APTES and hydroxylated $nTiO_2$/Ti surface (Que et al., 2000). The peaks founds at 1560, 1633 and 3350 cm^{-1} are assigned to bending and stretching vibration of the –N–H bond resulting from amine ($–NH_2$) groups presence on $nTiO_2$/Ti surface (Tasviri et al., 2001). Further, the peaks observed at 2933, 2874 and 1460 cm^{-1} are attributed to stretching and bending vibration of the –C–H bond. In case of Tyrs–APTES/TiO_2/Ti film (curve c), the peaks observed at 1230 cm^{-1} and 1277 cm^{-1} correspond to the –C=N stretching vibration of amide. The peaks at 1536 and 1652 cm^{-1} are attributed to the NH bending in carbonyl amide bond. This study confirms the surface functionalization of $nTiO_2$/Ti film with APTES and Tyrs.

3.2. Surface morphological studies

The morphological investigation of Ti and $nTiO_2$ films was carried out using AFM (Fig. 2). Micrograph shows a uniform spread of Ti nanoparticles onto glass substrate. The average size of these spherical Ti particles is calculated as 102 nm with average film roughness 3.44 nm and shown in a histogram plot [Fig. 2(v)]. Size homogeneity of the Ti particles arises due to uniform deposition resulting in well structured film formation. Magnified image of Ti particles and 3D image are shown in inset of Fig. 2(i) and (iii), respectively. After electrochemical oxidation of Ti film, the changes can be observed in the grain size distribution of the $nTiO_2$ film (image ii). The $nTiO_2$ film and 3D image are shown in inset of Fig. 2 (ii, magnified image) and (iv), respectively. A histogram plot shows the particles size distribution of $nTiO_2$ and the average size is estimated as 28 nm [Fig. 2(vi)]. The average roughness of $nTiO_2$ film has been found to be 4.84 nm. Silanization of $nTiO_2$ film surface led to increased average thickness of this nanostructured electrode as a result of SAM formation due to covalently attached APTES. The significant rises in the film roughness (63.2 nm) confirm APTES modification on $nTiO_2$ film. After the immobilization of Tyrs, the surface morphology of $nTiO_2$ film is changed into an uneven surface with increased value of average roughness (128 nm) confirming Tyrs adsorption onto APTES-$nTiO_2$/Ti surface.

In order to confirm the morphological shape of Ti and $nTiO_2$ particles and surface functionalization, we have carried out the scanning electron microscope (SEM) studies. The SEM image of DC sputtered Ti substrate shows a uniform and homogeneous surface (Fig. 3(i)). It has been seen that the Ti particles are spherical and closely packed. The oxidized Ti film is shown in Fig. 3(ii). It has been observed that porous $nTiO_2$ particles have globular 3D structures. The oxidized surface of Ti film has irregular grains compared to sputtered Ti surface. The electrochemical oxidation leads to asymmetrical patches or trenches on the film surface (ii and iii) which may useful for surface functionalization (Oliveira et al., 2007; Weetall and Hersh, 1970). Further, the oxidized $nTiO_2$ surface was functionalized with positively charged APTES and GA [image 3(iv)] (Tasviri et al., 2001). GA reacts with amino groups of the silanized surface for binding of enzyme molecules. Fig. 3(iv) shows APTES and GA layer on $nTiO_2$ surface. After enzyme immobilization, a morphological change of Tyrs–APTES/$nTiO_2$/Ti surface has been observed [image 3(v)] due to the covalent interaction of GA and enzyme. The elemental (EDAX) analysis of $nTiO_2$ film has been conducted to investigate the atomic ratio and % weight of Ti and O [Fig. 3(vi)]. This study confirms the presence of oxygen and Ti elements in $nTiO_2$ film. Contact angle measurements have been carried out to confirm the hydrophilic nature of the film surfaces at various stages of electrode fabrication (Fig. S2, Supplementary data).

3.3. Electrochemical studies

To investigate the interfacial properties of various electrodes, we have conducted the electrochemical impedance spectroscopy (EIS). The electrochemical impedance can be represented as the sum of the real (Z') and imaginary (Z'') components that mainly originate from the resistance and capacitance of the electrochemical cell. Fig. 4 shows the EIS spectra of various electrodes as a function of frequency (0.01–10^5 Hz) at a bias potential of 0.01 V [Fig. 4(i)]. The charge transfer resistance (R_{CT}) value calculated from semicircular region for $nTiO_2$/Ti electrode (290 kΩ, curve b) is higher compared to that of bare Ti electrode (106 kΩ, curve a). This is due to the formation of $nTiO_2$ semiconducting particles via oxidation which obstruct the electron transfer from electrolyte to electrode. Further, APTES and GA modification on $nTiO_2$/Ti surface increases the R_{CT} value (435 kΩ, curve c) due to presence of available functional groups ($–NH_2$ and –CHO) on electrode surface.

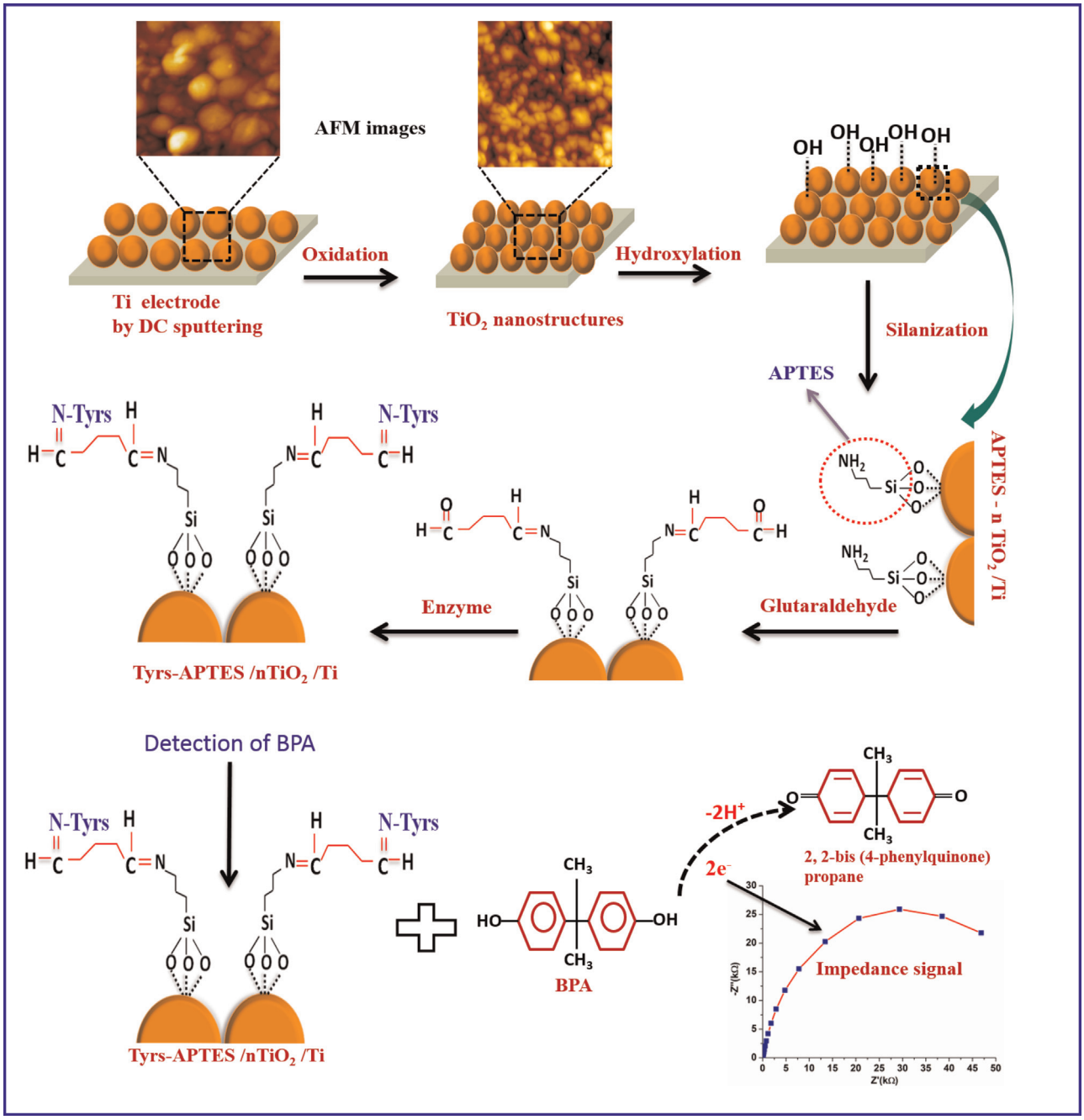

Scheme 1. Self assembled DC sputtered nanostructured rutile TiO_2 platform detection of estrogenic substance.

Moreover, the SAM formation of APTES can arrange $nTiO_2$ nanoparticles suitably on electrode surface and provide a better conformation for enzyme immobilization. The R_{CT} value of Tyrs–APTES/$nTiO_2$/Ti bioelectrode [Fig. 4(i)d] has found to be large (462 kΩ) compared to that of the APTES-$nTiO_2$/Ti electrode. This large R_{CT} value of enzymatic electrode is because of the insulating nature of tyrosinase molecules which covalently binds with APTES via cross linker. The amount of enzyme immobilization has been optimized at 10 μl where the R_{CT} value is found to be maximum response. Surface coverage of $nTiO_2$/Ti, APTES-$nTiO_2$/Ti and Tyrs–APTES/$nTiO_2$/Ti electrodes were calculated as 44%, 75% and 77%, respectively, using the relation as reported literature (Ali et al., 2014).

The cyclic voltammetry (CV) studies have been conducted to investigate the electrochemical properties of the various electrodes in the potential range of −1.5 to 0.5 V at a scan rate of 10 mV/s [Fig. 4(ii)]. The increase in oxidation current of $nTiO_2$/Ti electrode (0.10 mA) [curve b, Fig. 4(ii)] after electrochemical oxidation of Ti electrode (0.012 mA) indicates larger surface area of TiO_2 nanoparticles which may improve electron transfer from electrolyte to electrode. Additionally, the presence of gibbosities and point detects on $nTiO_2$ surface facilitates the charge transfer between enzyme and electrode (Li et al., 2012). In curve c, the APTES-$nTiO_2$/Ti electrode shows further declination in current response (0.03 mA) due to SAM formation on $nTiO_2$/Ti particles. Interestingly, after immobilization of Tyrs enzyme, the electrode shows a maximum

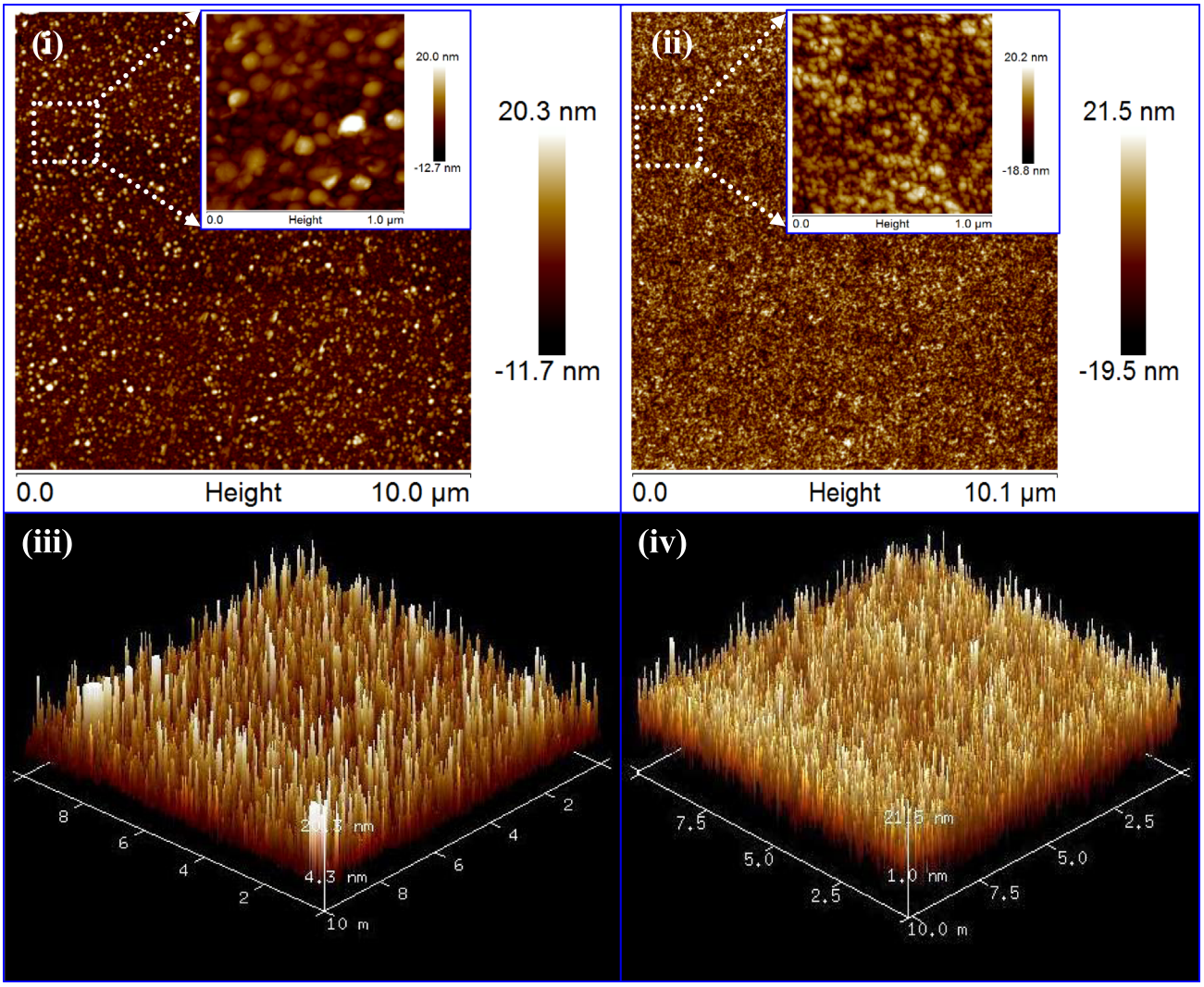

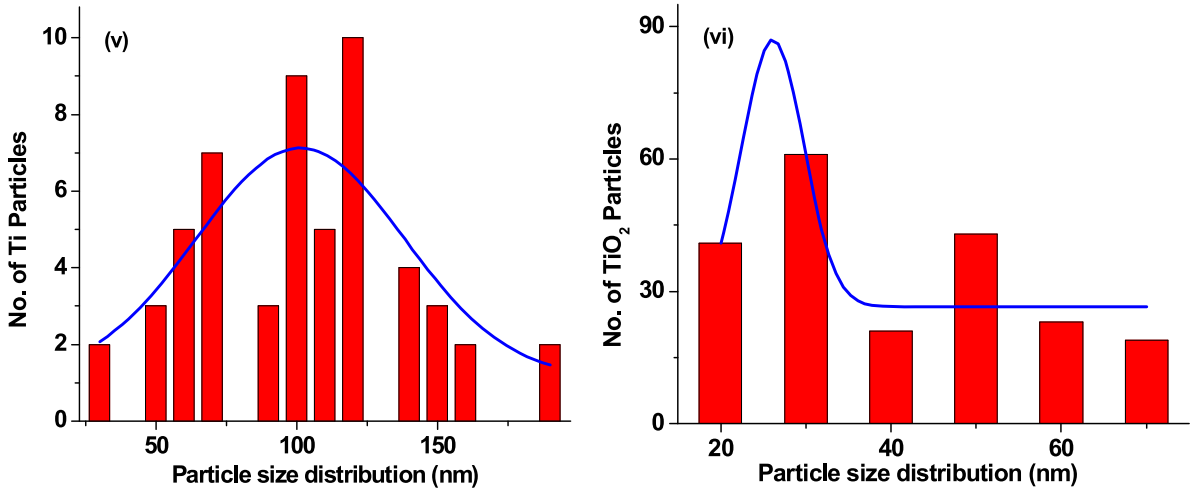

Fig. 2. (i) AFM images of Ti film, inset zoom image of Ti film, (ii) AFM images of $nTiO_2$ film, inset zoom image of $nTiO_2$ film, (iii) 3D image of Ti film, (iv) 3D image of $nTiO_2$ film, (v) and (vi) histogram plots for average size of Ti and $nTiO_2$ particles, respectively.

current response of 0.14 mA compared to other films. This may be attributed to covalently bonded APTES on $nTiO_2$/Ti electrode provides a favorable conformational environment for Tyrs. The available active sites on Tyrs may electrochemically activate in presence $nTiO_2$ particles and these $nTiO_2$ particles mediated the generated electrons from redox reaction toward the electrode (Ali et al., 2012; Li et al., 2012). The CV studies of Tyrs–APTES/$nTiO_2$/Ti bioelectrode have been conducted as a function of scan rate [Fig. S3, Supplementary data]. The anodic peak currents show linear variation with square root of the scan rate [Fig. S3, inset (i)], suggesting that the reaction at electrode is the diffusion controlled process and obeys the following anodic Eq. (1):

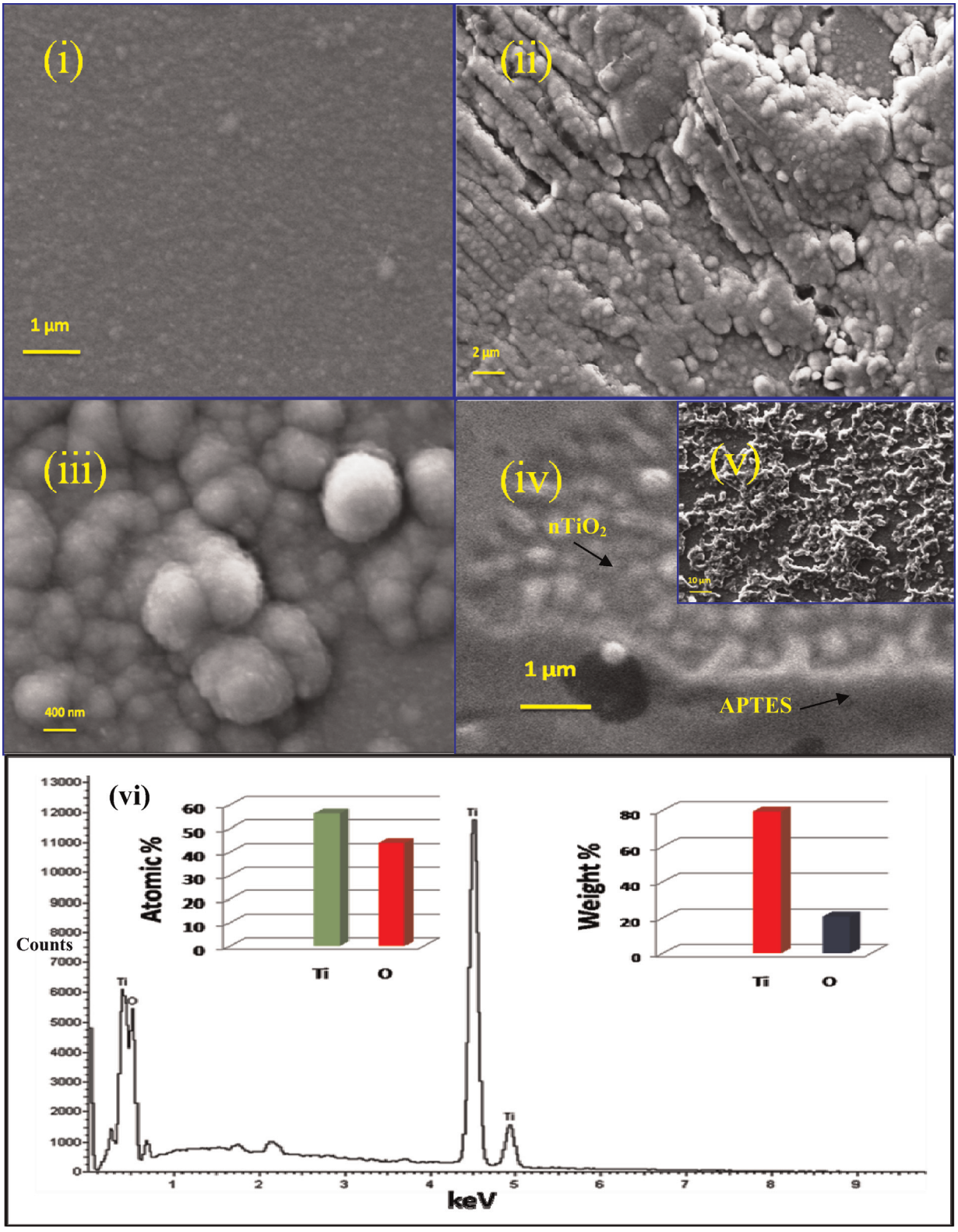

Fig. 3. (i) SEM image of Ti electrode, (ii and iii) $nTiO_2$/Ti electrode, (iv) APTES-$nTiO_2$/Ti electrode, (v) Tyrs–APTES/$nTiO_2$/Ti bioelectrode after Tyrs immobilization and (vi) elemental analysis (EDAX) image of $nTiO_2$/Ti electrode.

$$I_A(\text{bioelectrode}) = 4.49\,\mu A - 1.17E \times 10^{-4}\left(A^2 mV^{-1} s\right)^{1/2} \times\left[\text{Scanrate}(mVs^{-1})\right]^{1/2};\quad r^2 = 0.967 \tag{1}$$

Fig. 4(iii) shows EIS spectra of Tyrs–APTES/nTiO$_2$/Ti bioelectrode as a function of potential (0.01–1.0 V). The R_{CT} value for this bioelectrode has been found to increase linearly with increasing potential. This reveals the superficial electron transfer kinetics of the redox probe for the Tyrs–APTES/nTiO$_2$/Ti bioelectrode. The electron transfer resistance can be translated into current under the equilibrium (I_0) and the heterogeneous electron-transfer rate constant (HET) can be estimated using Eqs. (2–4).

$$R_{CT} = RT/nFI_0 \tag{2}$$

$$I_0 = n\text{FAHET}[S] \tag{3}$$

$$\text{HET} = RT/n^2F^2AR_{CT}[S] \tag{4}$$

where R is gas constant, T is absolute temperature (K), F is Faraday constant, A is the electrode area (cm^2), [S] is the bulk concentration of redox probe (mol cm^{-3}) and n is the number of transferred electrons per molecule of the redox probe. The values of HET for Ti, nTiO$_2$/Ti, APTES-nTiO$_2$/Ti and Tyrs–APTES/nTiO$_2$/Ti electrodes are 1.01 μcm s^{-1}, 0.36 μcm s^{-1}, 0.246 μcm s^{-1} and 0.231 μcm s^{-1}, respectively.

The pH of the buffer solution may affect the charge transfer properties of an enzyme immobilized APTES-nTiO$_2$/Ti bioelectrode. Impedance of this bioelectrode in different pH solutions was measured to investigate the charge transfer properties between electrode and electrolyte. Fig. 4(iv) shows the EIS spectra for the Tyrs–APTES/nTiO$_2$/Ti bioelectrode with different pH (5.5–8.0) values containing 1.0 μM of BPA at room temperature (27 °C). The R_{CT} value decreases with increasing the pH value (5.5–8.0) of electrolyte solution. The R_{CT} value of bioelectrode is saturated at pH 7.4. This may be due to Tyrs retain their natural structure and do not get denatured (Amine et al., 2006) further with increase in pH. The histogram shows the variation of obtained R_{CT} with different pH [inset: Fig. 4(iv)]. Thus, the pH value of 7.4 was chosen for all studies relating to electrochemical activity and BPA biosensing.

3.4. Detection of bisphenol A

The EIS response for Tyrs–APTES/nTiO$_2$/Ti bioelectrode has been investigated [Fig. 5(i)] in presence of various BPA

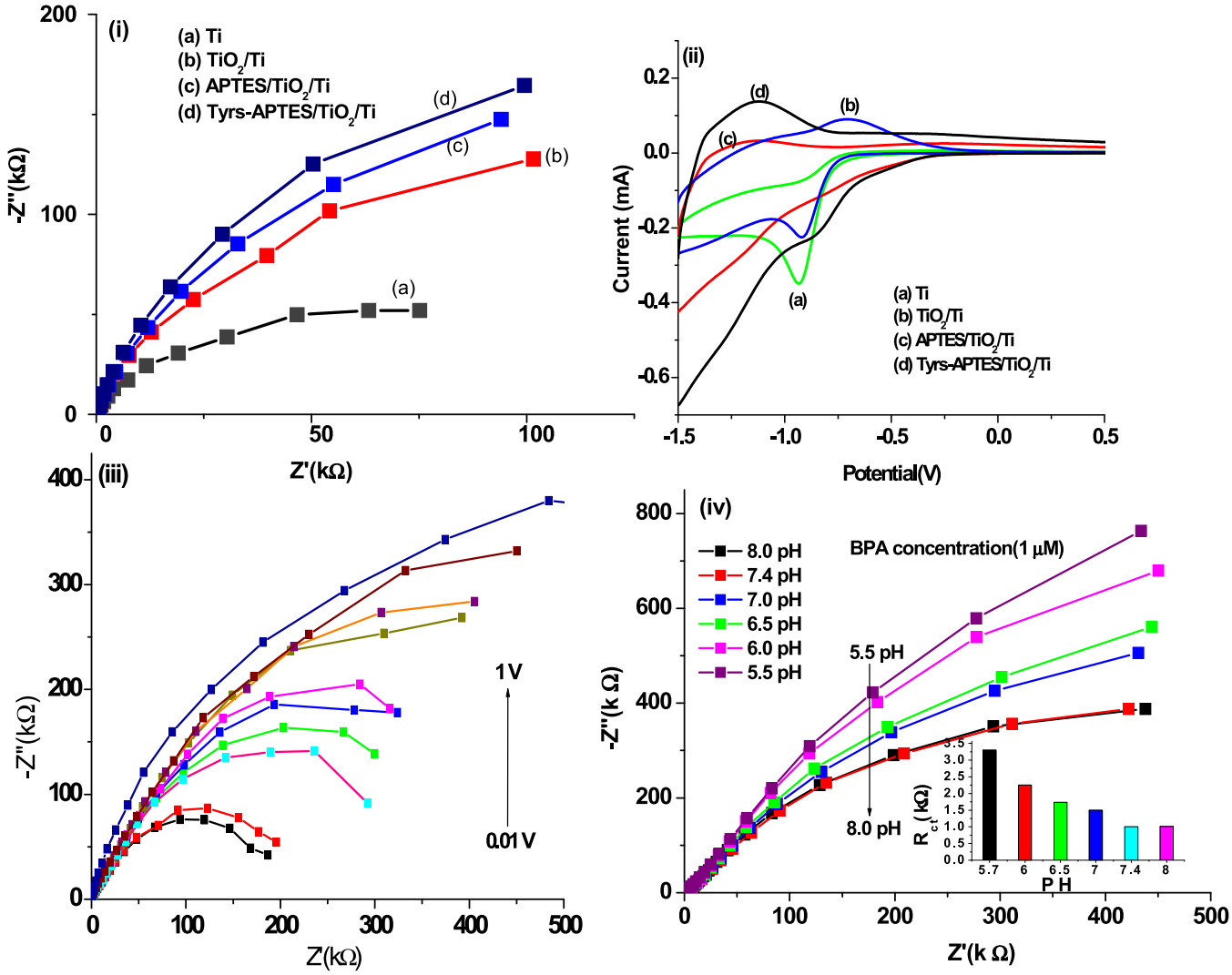

Fig. 4. (i) Electrochemical impedance spectroscopy(EIS) spectra of, Ti electrode (a), nTiO$_2$/Ti electrode (b), APTES-nTiO$_2$/Ti electrode (c), and Tyrs–APTES/nTiO$_2$/Ti bioelectrode (d) in PBS (50 mM, pH 7.4) solution containing 5 mM $[Fe(CN)_6]^{3-/4-}$. (ii) The cyclic voltammogram of, Ti electrode (a), nTiO$_2$/Ti electrode (b), APTES-nTiO$_2$/Ti electrode (c), and Tyrs–APTES/nTiO$_2$/Ti bioelectrode (d). (iii) EIS spectra of Tyrs–APTES/nTiO$_2$/Ti bioelectrode as a function of potential (0.01–1.0 V). (iv) EIS spectra for the Tyrs–APTES/nTiO$_2$/Ti bioelectrode in 50 mM PBS with different pH values (5.5–8.0).

concentration (0.01–1.0 μM). The change in R_{CT} is observed at different concentrations of BPA as shown in Fig. 5(i). This was attributed to the presence of Tyrs on APTES-nTiO_2/Ti surface, which converts BPA into 2,2-bis(4-phenylquinone) propane. In enzymatic reaction, the generated electrons during the oxidation of BPA are transferred to nTiO_2/Ti electrode through electrolytic solution resulting in decreased value of R_{CT}. Thus, other than mediator electrons, the change in the R_{CT} value during BPA detection is arising from generation of electrons during enzymatic reaction. A linear relationship between change in R_{CT} and concentration of BPA (0.01–1.0 μM) has been observed [Fig. 5(ii)] with best fitting to the linear regression equation of R_{CT} (kΩ)=411.7–361.9 kΩ × BPA (μM) with a correlation coefficient (R^2) of 0.993. It has been observed from Fig. 5 that the Tyrs–APTES/nTiO_2/Ti biosensor shows a low limit of detection (0.01 μM), a fast response time (250 s) and a sensitivity of 361.9 kΩ/μM in a wide range of concentrations (0.01–1.0 μM). The sensitivity of this fabricated biosensor is 88 times higher compared to the biosensor based on molecular imprinted polymer film (Apodaca et al., 2011). A comparable sensitivity of this biosensor compared to those reported literature (Table S1) may be due to higher electron transfer properties arising from surface defects and oxygen vacancies of rutile nTiO_2 particles and its strong covalent interaction with Tyrs molecules. In addition, this may be due to surface functionalization of APTES onto the nTiO_2/Ti electrode surface. The biosensing characteristics of Tyrs–APTES/nTiO_2/Ti bioelectrode along with those reported in literature have been summarized in Table S1 (Supplementary data). The prepared biosensor show a low detection limit of 0.01 μM which is lower than other reported in literature (Huang et al., 2011; Li et al., 2012). This may be due to the presence of point defects in nTiO_2 which enhances the loading capacity of Tyrs molecules. Fig. S4 (Supplementary data) shows a plot between real component of impedance signal and log of frequency. The value of the Michaelis–Menten constant (K_m) is obtained to be 0.023 μM. This low value to K_m indicates that the Tyrs–APTES/nTiO_2/Ti matrix have strong affinity with BPA molecules and facilitates enzymatic reaction resulting in enhanced enzymatic activity. The preparation procedure of this biosensor is more practical and safer as we used SAM and glutaraldehyde for functionalization compared to Zhou et al. (2012) where HF has been used. The control

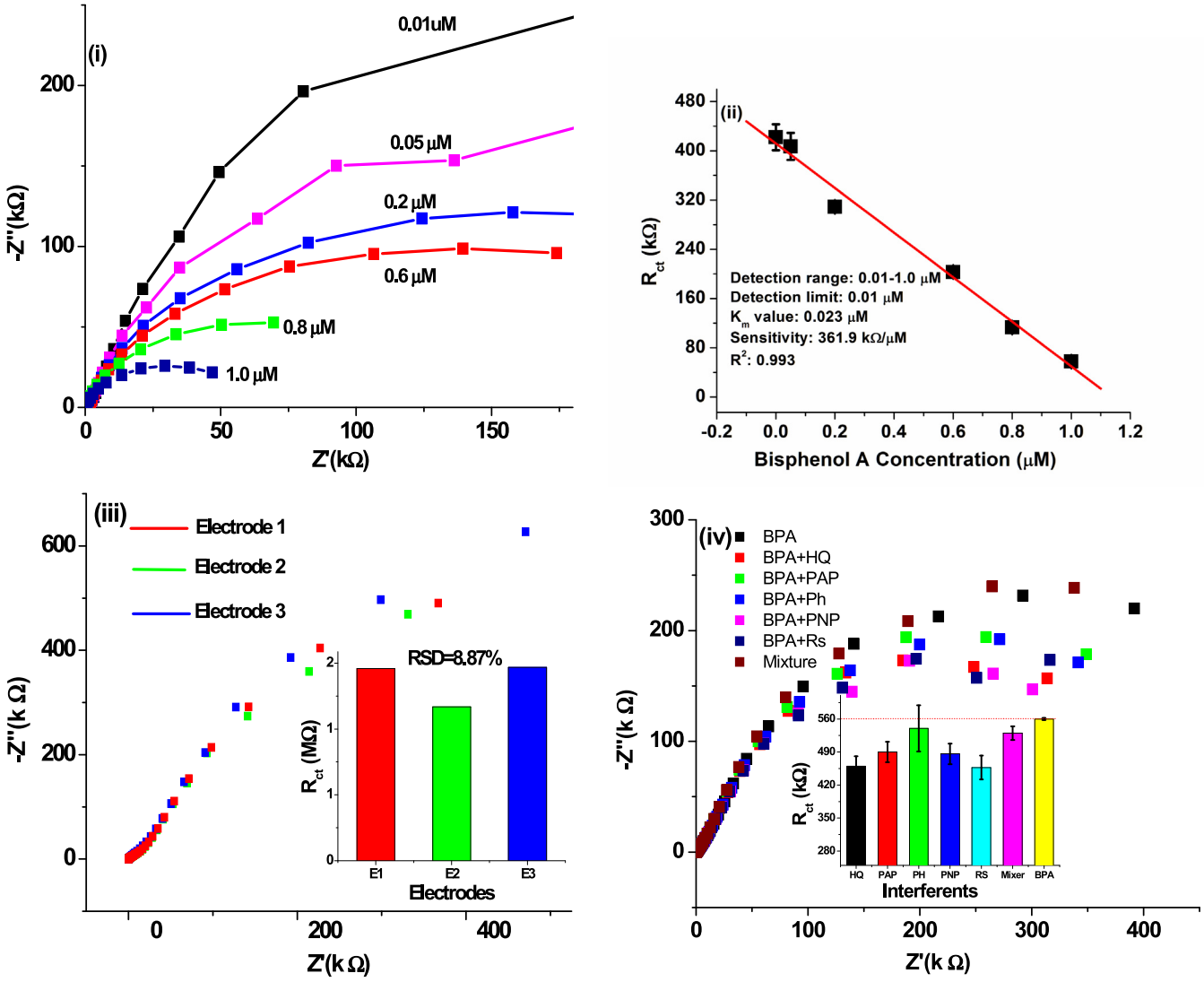

Fig. 5. (i) EIS spectra of Tyrs–APTES/nTiO_2/Ti bioelectrode as a function of bisphenol A concentration (0.01–1.0 μM) in PBS solution containing 5 mM $[Fe(CN)_6]^{3-/4-}$, (ii) calibration curve between R_{CT} value and bisphenol A concentration (μM), (iii) reproducibility of Tyrs–APTES/nTiO_2/Ti bioelectrode, and (iv) the selectivity of Tyrs–APTES/nTiO_2/Ti bioelectrode.

experiments for $nTiO_2$/Ti electrode with and without Tyrs immobilization have been conducted using EIS technique [Fig. S5(i and ii)]. It has been found that there is small change in R_{CT} value in the response signal of prepared electrode for BPA detection without immobilizing enzyme. The small change in the control studies of $nTiO_2$/Ti electrode may be due to noise or non-specific reaction with proteins. The enzyme can play a significant role for detection of BPA in the real sample analysis Fig. S5(iii). The prepared biosensor has been carried out in presence of real samples with varying BPA concentration. In comparison to the standard BPA concentration, it has been observed that the bioelectrode shows a difference at low BPA concentration other than higher concentration of BPA detection.

The reproducibility of Tyrs–APTES/$nTiO_2$/Ti bioelectrode [Fig. 5 (iii)] has been investigated at 0.2 μM of BPA concentration. No significant change in the R_{CT} value has observed after 10 times repeated measurements as evident by low relative standard deviation (RSD=8.87%). The selectivity of Tyrs–APTES/$nTiO_2$/Ti bioelectrode [Fig. 5(iv)] has been estimated in presence of BPA (1.0 μM) concentration with normal concentration of interferents such as phenol (1.0 μM), para-nitrophenol (1.0 μM), para-aminophenol (0.8 mM), resorcinol (1.0 μM), hydroquinone (0.8 μM), and all mixers [Fig. 5(iv)]. The Tyrs–APTES/$nTiO_2$/Ti bioelectrode is not significantly affected in the presence of interferents during BPA detection. The R_{CT} value remains nearly same except for resorcinol and hydroquinone wherein there is a decrease of R_{CT} about 20%. The absorption of available hydroxyl groups on transducer surface may decrease value of R_{CT}. The stability of the Tyrs–APTES/$nTiO_2$/Ti bioelectrode has been checked for 8 weeks as an interval of 1 week. The increase in the value of R_{CT} has been found to be about 10% up to 4 weeks after which the R_{CT} value is increased 40% within 10 weeks.

4. Conclusion

A cheap, easy, reproducible and sensitive nTO_2 based biosensor platform for detection of BPA has been demonstrated. We have synthesized a low temperature process nanocrystalline Ti film on glass substrate by DC sputtering technique. Ti surface on glass has been converted to $nTiO_2$ via electrochemical oxidation in presence of HF and ethylene glycol. Nanocrystalline Ti surface has been controlled by varying deposition time, deposition vacuum and deposition voltage. Low temperature synthesis process of rutile $nTiO_2$/Ti film has been utilized for the detection of BPA concentration. The surface functionalization of monodisperse $nTiO_2$ particles with APTES and GA improve the loading capacity of Tyrs enzyme molecules. SAM of APTES has been treated on rutile $nTiO_2$/Ti film surface to perform a cross link with GA molecules for Tyrs enzyme functionalization. The covalent interaction between Tyrs enzyme and APTES on $nTiO_2$/Ti electrode results in improved sensing characteristic for monitoring BPA concentration. This fabricated biosensor exhibits a sensitivity (361.9 kΩ/μM) in a wide detection range (0.01–.0 μM). The $nTiO_2$ based biosensor is provided a safer platform for excellent electrochemical sensing parameters due to integration APTES and Tyrs. This biosensor shows excellent selectivity, fast detection and good reproducibility. This biosensor is sensitive to 0.01 μM concentration of BPA due to the presence of point defect in rutile TiO_2 nanoparticles which improve the charge transfer properties between electrode and electrolyte. This biosensor platform could be utilized for monitoring other clinical substances such as low density lipoprotein, glucose, leukemia, etc.

Acknowledgements

We thank Director NPL, New Delhi, India for the facilities. We thank Rachna Sharma, NPL for AFM measurements. Ved Varun Agrawal is thankful to CSIR Empower project (OLP 102332) for funding. The financial support received from Department of Science and Technology, Ministry of Science and Technology, India (Grant no. DST/TSG/ME/2008/18) is gratefully acknowledged.

Appendix A. Supplementary material

Supplementary data associated with this article can be found in the online version at http://dx.doi.org/10.1016/j.bios.2015.01.041.

References

Ali, M.A., Srivastava, S., Solanki, P.R., Agrawal, V.V., John, R., Malhotra, B.D., 2012. Appl. Phys. Lett. 101, 084105.
Ali, M.A., Srivastava, S., Mondal, K., Chavhan, P.M., Agrawal, V.V., John, R., Sharma, A., Malhotra, B.D., 2014. Nanoscale 22, 13958–13969.
Alkasir, R.S.J., Ganesana, M., Won, Y.H., Stanciu, L., Andreescu, S., 2010. Biosens. Bioelectron. 26, 43–49.
Amine, A., Mohammadi, H., Bourais, I., Palleschi, G., 2006. Biosens. Bioelectron. 21, 1405–1423.
Apodaca, D.C., Pernites, R.B., Ponnapati, R., Del Mundo, F.R., Advincula, R.C., 2011. Macromolecules 44, 6669–6682.
Berger, T., Lana-Villarreal, T., Monllor-Satoca, D., Gomez, R., 2007. J. Phys. Chem. C 111, 9936–9942.
Brown, S.A., Lemons, J.E., 1996. Medical applications of titanium and its alloys: the material and biological issues, ASTM International.
Di Valentin, C., Pacchioni, G., Selloni, A., 2006. Phys. Rev. Lett. 97, 166803.
Duenas, S., Castaˇn, H., Garcia, H., San Andres, E., Toledano-Luque, M., Maˇrtil, I., Gonzalez-Diaz, G., Kukli, K., Uustare, T., Aarik, J., 2005. Semicond. Sci. Technol. 20, 1044.
Dunn, D.N., Hull, R., Ross, F.M., Tromp, R.M., 2001. J. Appl. Phys. 89, 2635–2640.
DiVall, S.A., 2013. Curr. Opin. Endocrinol. Diabetes Obes. 20, 50–55.
Guillemot, F., Porte, M.C., Labrugere, C., Baquey, C., 2002. J. Colloid Interface Sci. 255, 75–78.
Hiroi, H., Tsutsumi, O., Momoeda, M., Takai, Y., Osuga, Y., Taketani, Y., 1999. Endocr. J. 46, 773–778.
Huang, J., Zhang, X., Liu, S., Lin, Q., He, X., Xing, X., Lian, W., 2011. J. Appl. Electrochem. 41, 1323–1328.
Kim, K.-H., Ramaswamy, N., 2009. Dent. Mater. J. 28, 20–36.
Kloas, W., Lutz, I., Einspanier, R., 1999. Sci. Total Environ. 225 (1), 59–68.
Li, Q., Cheng, K., Weng, W., Du, P., Han, G., 2012. J. Mater. Chem. 22, 9019–9026.
Li, X., Huang, F., Curry, M., Street, S.C., Weaver, M.L., 2005. Tribol. Lett. 19, 273–280.
Ntsendwana, B., Mamba, B.B., Sampath, S., Arotiba, O.A., 2012. Int. J. Electrochem. Sci. 7, 3501–3512.
Oliveira, E.M., Beyer, S., Heinze, J., 2007. Bioelectrochemistry 71, 186–191.
Que, W., Zhou, Y., Lam, Y.L., Chan, Y.C., Kam, C.H., 2000. Thin Sol. Films 358, 16–21.
Reza, K.K., Singh, N., Yadav, S.K., Singh, M.K., Biradar, A.M., 2014. Biosens. Bioelectron. 62, 47–51.
Sohoni, P., Tyler, C.R., Hurd, K., Caunter, J., Hetheridge, M., Williams, T., Woods, C., Evans, M., Toy, R., Gargas, M., 2001. Environ. Sci. Technol. 35, 2917–2925.
Steinmetz, R., Brown, N.G., Allen, D.L., Bigsby, R.M., Ben-Jonathan, N., 1997. Endocrinology 138 (5), 1780–1786.
Tasviri, M., Rafiee-Pour, H.-A., Ghourchian, H., Gholami, M.R., 2001. Appl. Nanosci. 1, 189–195.
Vandenberg, L.N., Colborn, T., Hayes, T.B., Heindel, J.J., Jacobs Jr., D.R., Lee, D.-H., Shioda, T., Soto, A.M., Saal, F.S. v, Welshons, W.V., Zoeller, R.T., Myers, J.P., 2012. Endocr. Rev. 33, 378–455.
Weetall, H.H., Hersh, L.S., 1970. Biochim. Biophys. Acta 206 (1), 54–60.
Wen, Y., Zhou, B.-S., Xu, Y., Jin, S.-W., Feng, Y.-Q., 2006. J. Chromatogr. A 1133 (1), 21–28.
Wang, G., Chen, Z., Bartell, T., Wang, X., 2014. Curr. Environ. Health Rep. 1, 78–89.
WHO, 2012. Endocrine Disrupters and Child Health.
Xiao, P., Zhang, Y., Cao, G., 2011. Sens. Actuators B—Chem. 155, 159–164.
Yin, H., Zhou, Y., Xu, J., Ai, S., Cui, L., Zhu, L., 2010. Anal. Chim. Acta 659, 144–150.
Zhou, Y., Huang, Y., Li, D., He, W.-h, Guo, C.-c, LU, C.-x, Zhang, S.-y., 2012. J. Cent. South Univ. 19, 2740–2745.